Embedding a Nonlinear Strict Oscillatory Mode into a Segmented Leg

Sesselmann, Anna; Loeffl, Florian; Santina, Cosimo Della; Roa, Maximo A.; Albu-Schaffer, Alin

DOI
10.1109/IROS51168.2021.9636605

Publication date
2021

Document Version
Final published version

Published in
Proceedings of the IEEE/RSJ International Conference on Intelligent Robots and Systems, IROS 2021

2021 IEEE/RSJ International Conference on Intelligent Robots and Systems (IROS)
September 27 - October 1, 2021. Prague, Czech Republic

2021 IEEE/RSJ International Conference on Intelligent Robots and Systems (IROS) | 978-1-6654-1714-3/21/$31.00 ©2021 IEEE | DOI: 10.1109/IROS51168.2021.9636605

Embedding a Nonlinear Strict Oscillatory Mode into a Segmented Leg

Anna Sesselmann[1] Florian Loeffl[1] Cosimo Della Santina[1,2] Maximo A. Roa[1] Alin Albu-Schäffer[1,3]

***Abstract*— Robotic legs often lag behind the performance of their biological counterparts. The inherent passive dynamics of natural legs largely influences the locomotion and can be abstracted through the spring-loaded inverted pendulum (SLIP) model. This model is often approximated in physical robotic legs using a leg with minimal mass. Our work aims to embed the SLIP dynamics by using a nonlinear strict oscillatory mode into a segmented robotic leg with significant mass, to minimize the control required for achieving periodic motions. For the first time, we provide a realization of a nonlinear oscillatory mode in a robotic leg prototype. This is achieved by decoupling the polar task dynamics and fulfilling the resulting conditions with the physical leg design. Extensive experiments validate that the robotic leg effectively embodies the strict mode. The decoupled leg-length dynamic is exhibited in leg configurations corresponding to the stance and flight phases of the locomotion task, both for the passive system and when actuating the motors. We additionally show that the leg retains this behavior while performing jumping in place experiments.**

I. Introduction

Quadrupedal mammals show more endurance when traveling and reach higher speeds than legged robots. It is commonly accepted that these capabilities are already embodied in the passive dynamics of the animal and are not only a result of the control [1]. Biology has provided substantial inspiration for legged robotics, especially in the case of (articulated) soft robotics [2], where passive elastic elements are added to the structure to replicate the dynamic properties of natural tendons [3], [4]. However, the natural performance of animals is still unmatched to a large extent.

The spring-loaded inverted pendulum (SLIP) template model and its many extensions to the bipedal and quadrupedal case (e.g. [5]) passively exhibit most gaits that are shown in nature. However, although being effective in describing animal behavior, the SLIP model neglects the complex interplay between inertial and elastic forces that occurs in a real segmented leg. The work of Abate [6] illustrates that two main challenges exist in designing SLIP-like robotic legs: the implementation of a decoupled elastic potential in task space, and the design of a rigid body mechanism free of undesired inertial couplings. Raibert's one-leg hopper [7] straightforwardly obtains a decoupled leg dynamics by utilizing a prismatic joint. Mechanisms implementing a decoupled elastic potential in articulated legs are proposed in [8]. Undesired inertial couplings are commonly minimized by simply reducing the total mass of the leg, as demonstrated in the design of current legged robots such as ATRIAS [9], Cheetah-cub [10], MIT Mini Cheetah [11], Cassie [12], or Spacebok [13]. Additionally, these robots incorporate elastic elements to store energy during locomotion. However, - contrary to the SLIP-model - the decoupling of the dynamics in the polar task space is not present in these robots, and complex control is needed to achieve this characteristic.

Fig. 1: Front and side view of the proposed articulated soft robotic leg prototype. We embed during the design phase a SLIP-like behavior when the leg is close to the vertical configuration. This is done by selecting suitable physical parameters in order to embed a vertical strict mode in the dynamics. As a result, the leg can efficiently jump in place exploiting its natural dynamics.

Our main idea in this paper is to have a robotic leg with fully decoupled dynamics in the polar task space to highly simplify the required control. We propose and test an articulated soft leg with non-negligible mass, to reproduce SLIP-like behavior. To this end, we look at modal analysis. The theory on nonlinear modes, recently extended to fit the robotics case [14]–[16], provides a sound and practical framework for bridging the gap between the SLIP template and a multi-body elastically actuated segmented leg. Based on this theory, we propose and design a segmented robotic leg with a pantograph mechanism [16]. We embed for the first time a strict mode of a similar kind to [15] along the radial axis of the leg. Leg properties are also chosen to be coherent with scale effects between overall mass and leg design present in quadrupedal mammals [17], [18]. Finally, parameters are optimized to maximize implementability.

We provide an optimal and realistic parameter specifica-

This project has received funding from the European Research Council (ERC) under the European Union's Horizon 2020 research and innovation programme with the grant agreement No 835284, M-Runner.

[1]Institute of Robotics and Mechatronics, German Aerospace Center (DLR), Wessling, Germany. Firstname.Lastname@dlr.de .

[2]Cognitive Robotics Department, Delft University of Technology, Delft, The Netherlands.

[3]Chair of Sensor Based Robotic Systems and Intelligent Assistance Systems, Department of Informatics, Technical University of Munich (TUM), München, Germany.

tion for this robotic leg. We build a leg prototype (Fig. 1) employing rapid prototyping techniques and system parameters are identified. We validate the decoupled strict mode design in different configurations and operation modes of the robot, including jumping. Our experiments validate the existence of the embodied nonlinear strict mode and the corresponding decoupled radial dynamics of the leg. Furthermore, the experiments show that the mode can be maintained using a simple bang-bang control. These results support our vision that robotic legs with intrinsic oscillatory modes are the first step towards template-based robotic locomotion with minimal control effort.

II. Problem Statement

A. Dynamic Model of the Pantographic Leg

Inspired by the natural example and based on the well-known capability of parallel mechanisms to implement dynamic decouplings, we consider as the basis of our design the three-segmented leg with a pantograph mechanism shown in Fig. 2a and 2b. In this section, we consider an ideal foot-floor interaction, modeled as a revolute joint. We also consider the rotation of the trunk to be blocked, to create a stable upright equilibrium position. These assumptions are only instrumental to deriving analytical solutions, and they will be relaxed when performing simulations and experiments.

The pantographic leg has two degrees of freedom (DoF). Its configuration space is $q = [q_1, q_2] \in \mathbb{R}^2$, where q_1 is the angle of the hip joint and q_2 is the one between the shank and the trunk (see Fig. 2b). The two joints are actuated through Series Elastic Actuators (SEAs). The two springs (shown in Fig. 2a) have stiffness k_1 and k_2. We consider to have perfect control on the motor side. Therefore, the motor angles $q_d \in \mathbb{R}^2$ will serve as control inputs.

The trunk has mass m_t, and the thigh, shank, and foot segments have masses m_i, lengths l_i, centers of mass (CoM) c_i, and inertia I_i^c with $i \in \{1, 2, 3\}$ (Fig. 2a). It is worth underlining that we are considering a very general distribution of mass (not the usual homogeneous bar links). These extra free design parameters will be important later in the paper.

The overall dynamics has the usual form

$$M(q)\ddot{q} + C(q, \dot{q})\dot{q} + g(q) = \begin{bmatrix} k_1(q_{d,1} - q_1) \\ k_2(q_{d,2} - q_2) \end{bmatrix}. \quad (1)$$

Inertia matrix $M(q) \in \mathbb{R}^{2\times2}$, Coriolis and centrifugal forces $C(q, \dot{q})\dot{q} \in \mathbb{R}^2$, and gravitational forces $g(q) \in \mathbb{R}^2$ are evaluated in the usual way, and are reported in Appendix I.

We consider here a simplifying constraint on the segment lengths $l_2 = l_1 + l_3$, which ensures a linear dependency of the polar angle x_1 on q. The polar coordinates — angle x_1 and distance x_2 — of the foot expressed w.r.t. the trunk are

$$x = f(q) = \begin{pmatrix} \frac{1}{2}q_1 + \frac{1}{2}q_2 \\ (l_1 + l_3)\sqrt{2\,(1 + \cos(q_2 - q_1))} \end{pmatrix}. \quad (2)$$

Note the nonlinear dependency of the leg length x_2 on q.

B. Nonlinear Oscillatory Modes

Current extensions of linear modal analysis to the nonlinear domain are discussed in [14]. In this work, we are interested in a particular kind of strict mode [15] called similar mode. We will look for them in task space x. The name of these families of oscillations is due to their geometrical resemblance to the linear case - i.e., their trajectories identify a one-dimensional subspace in the configuration space. Consider the subspace $\mathrm{Span}\{w\}$, with $w \in \mathbb{R}^2$ being a unitary vector. We say that this subspace identifies a similar mode if for all initial conditions $[x, \dot{x}] = [w\xi(0), w\dot{\xi}(0)]$ for some $\xi(0), \dot{\xi}(0) \in \mathbb{R}$, then a full evolution

$$x(t) = w\,\xi(t) \quad (3)$$

exists, which is a solution of (1).

C. Problem Statement

Our goal is to derive a complete set of physical parameters for (1) that correspond to a strict similar mode and are compatible with a real leg design, without relying on conceptual simplifications such as massless segments. The design will be implemented for a 4kg quadruped similar to the DLR robot Bert [19]. We build and demonstrate the effectiveness of such a leg in the experimental section of the paper. This set of parameters should be such that (i) the similar mode $w = [0, 1]$ is embedded into the robot's dynamics; and to the extent that it is permitted by the kinematics and the segment-length constraint (ii) the leg should have geometrical and dynamical characteristics akin to a biological leg of a 4kg quadrupedal mammal.

III. Methods

This section describes the methods that we developed to achieve the desired goal. First, we ensure that the modal matching exists through analytical reasoning. As a result, a subset of free parameters is identified. Then we apply extra algebraic constraints to obtain a design that is close to the animal example. Finally, we explore the remaining parameter space via numerical optimization to maximize an index of physical implementability.

A. Modal Matching

The *Modal Matching* procedure discussed in this subsection extends the one introduced in [16]. Only homogeneous links shaped as a simple bar were considered there. That assumption simplified the analysis but also limited the type of behaviors that could be implemented.

Since we take w pointing in the direction of x_2 (radial motion), implementing the strict mode (3) is equivalent to decoupling the two equations in (1), whenever $x = [0, x_2]$ and $\dot{x} = [0, \dot{x}_2]$. A sufficient condition for achieving this goal is that all single elements in (1) are decoupled. The condition can also be proved to be necessary, but this is not a main interest for this paper (see [20] for a discussion of strict modes in the non-conservative case). It is worth noting that as a result of this procedure, we will end up with a

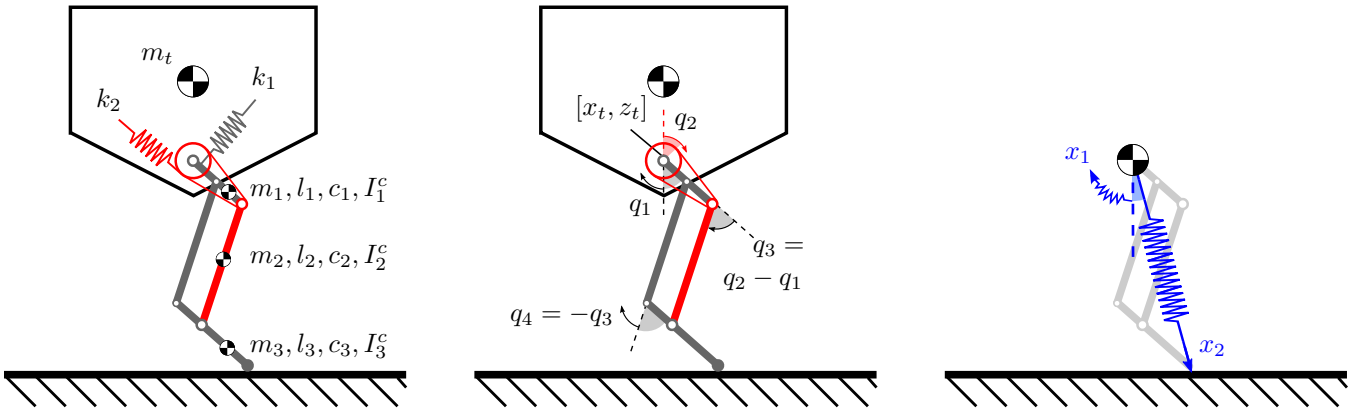

Fig. 2: Schematics of the three-segmented pantograph leg in comparison with the SLIP model. (a) The trunk has mass m_t, and the thigh, shank, and foot segments have masses m_i, lengths l_i, CoM c_i, and inertia I_i^c with $i \in \{1, 2, 3\}$. The springs have stiffness k_1 and k_2, and the elastic potential is $U_e = \sum_{i=1}^{2} k_i (q_{d,i} - q_i)^2/2$. (b) The position of the trunk at the hip joint is given by $[x_t, z_t]$. The angles of the hip q_1 and pulley q_2 fully determine the angles of the knee q_3 and ankle q_4. (c) The SLIP model can be described with the polar coordinates x. The springs are assumed to be in resting position at $x_1 = 0$ (vertical position) and $x_2 = l_o$.

system that behaves as the SLIP model locally around the vertical axis (Fig. 2c).

We start by imposing that the acceleration $\ddot{x}_2$ in the radial direction does not contribute to inertial forces in the polar direction. This is satisfied if the leg's task inertia is diagonal for all $x_1 = 0$. This in turn implies that the Coriolis and centrifugal task forces C_x are decoupled as well. Thus, we impose the condition — sufficient due to symmetry —

$$[0\ 1]\, J^{-T}\, M\, J^{-1}\, [1\ 0]^T = 0, \quad \forall x = [0, x_2]. \tag{4}$$

where $J = \partial x / \partial [q_1, q_2]$. It can be solved by the choice of parameters

$$\begin{aligned} 0 = {} & 2(c_1 m_1) l_3 + m_2 (l_1 + l_3)^2 - 2 c_2 m_2 (l_1 + l_3) \\ & + 2 c_1 m_1 l_1 - (m_2 + m_3) l_3^2 + 2 c_3 m_3 l_3) \\ & + m_2 c_2^2 + I_2 - m_1 c_1^2 - m_3 c_3^2 - I_1 - I_3. \end{aligned} \tag{5}$$

The detailed derivation of (4) is given in Appendix II. Second, we impose decoupling in elastic forces

$$[1\ 0]\, J^{-T} \begin{bmatrix} k_1 (q_{d,1} - q_1) \\ k_2 (q_{d,2} - q_2) \end{bmatrix} = 0, \quad \forall x = [0, x_2]. \tag{6}$$

This is solved by the following choice of parameters

$$k_1 = k_2. \tag{7}$$

Note that we do not explicitly consider here the damped case. However, in practice friction comes from bearings, and therefore in SEA actuators it tends to be aligned with the stiffness. In consequence, we expect damping forces to be decoupled as well. We experimentally test this hypothesis later in the paper.

Finally, we need to decouple gravitational forces

$$[1\ 0]\, J^{-T}\, g(q) = 0, \quad \forall x = [0, x_2], \tag{8}$$

which is solved by all parameters verifying

$$m_1 c_1 + m_3 (l_3 - c_3) = m_2 (l_1 - c_2). \tag{9}$$

B. Biological Plausibility

Besides the conditions presented in III-A, we impose biological similarity by adding constraints on overall leg properties, We impose the total mass to be $m_{\text{sys}} = 1\,\text{kg}$, calculated as a quarter of the total mass of the quadruped. From [18] it follows that a 4kg quadruped likely has leg mass $m_{\text{leg}} = 0.36\,\text{kg}$, leg CoM distance from the hip $c_{\text{leg}} = 0.068\,\text{m}$, and a relaxed leg length $l_o = 0.253\,\text{m}$. An indicative leg stiffness is $k_{\text{leg}}(l_o) = 905\,\text{Nm}^{-1}$ [17], which we can only define for a given leg length, as the radial stiffness of our model is nonlinear.

C. Physical Plausibility

Of the total of 15 free design parameters of the system (Fig. 2a), the modal matching specifies 4, and the additional condition inspired by biology specifies other 4. This leaves a set of 7 free parameters that we choose with the help of an optimization algorithm.

First, we normalize the seven free parameters in order to avoid bad conditioning of the problem (Table I). We obtain values that are feasible for the mechanical design by choosing the bounds considering that i) the relaxed leg length l_o should leave sufficient compression space in stance, ii) the segment CoMs c_i should be in the upper half of each segment l_i, and iii) the segments should have roughly stick-like inertias. Additionally, we ensure having a polar task stiffness that supports balancing the trunk, by solving

$$0 < \partial (\tau_{x_1} - g_{x_1}) / \partial x_1 \tag{10}$$

at the upright leg position $x_1 = 0$ for $k_{x_1} = \partial \tau / \partial x$, i.e. the stiffness is positive along the mode. In this way the mode has a stable equilibrium. The objective function is

$$\sum_{i=1}^{3} \left(\frac{m_i}{m_{\text{leg}}} - \frac{l_i}{l_1 + l_2 + l_3} \right)^2 + \frac{1}{2} \left(\frac{I_1}{m_1 l_1^2} - \frac{1}{12} \right)^2. \tag{11}$$

The first element favors longer segments to be heavier. This should allow the design of the whole leg using a single

TABLE I: Decision variables with their upper and lower bound. All variables are dimensionless.

Ratio	$\frac{l_o}{l_1+l_2+l_3}$	$\frac{l_1}{l_2}$	$\frac{c_1}{l_1}$	$\frac{c_2}{l_2}$	$\frac{c_3}{l_3}$	$\frac{I_2}{m_2\,l_2^2}$	$\frac{I_3}{m_3\,l_3^2}$
Lower	0.6	0.1	0.15	0.15	0.15	$1/16$	$1/16$
Default	0.8	0.6	0.45	0.45	0.45	$1/12$	$1/12$
Upper	0.95	0.9	0.5	0.5	0.5	$1/2$	$1/2$

material. If this constraint was not in place, we should have considered materials of different densities for each leg. The second element of the objective function favors simple stick-like inertia for the thigh.

IV. Model Parameters and Simulations

We use the evolutionary algorithm CMA-ES [21] to solve the nonlinear optimization problem. The algebraic equations derived in the previous subsections are then applied to obtain a complete set of optimal parameters. The result is shown in Table II.

A. Simulation

We use a fully hybrid system to simulate the leg. Besides the two angles q_1 and q_2, we add here the 2D position of the floating base. The rotation angle of the body is kept fixed. Therefore $q = [x_t, z_t, q_1, q_2]$, where $[x_t, z_t]$ gives the position of the trunk. We do not report here the full dynamic equations for the sake of space, but they are a direct generalization of the ones discussed so far. Interestingly, the decoupling conditions are still verified for this system.

The contact forces $f_c(q) = J_c^T(q)\,\lambda(q) \in \mathbb{R}^4$ map the Cartesian foot contact forces $\lambda(q)$ using the contact Jacobian $J_c(q)$ into the joint space. They are zero if the system is not in contact with the ground. The system is in flight phase if the vertical foot position is larger than zero. In touchdown, an updating rule based on the conservation of momentum is considered

$$\dot{q}^+ = (I - M^{-1}\,J_c^T\,(J_c\,M^{-1}\,J_c^T)^{-1}\,J_c)\,\dot{q}^- \qquad (12)$$

where the contact Jacobian J_c is used to account for the energy loss, by relating the velocities before and after the impact. The system is in contact with the ground (stance phase) until the vertical contact force in the footpoint becomes zero. We use `MATLAB`'s ode45 solver to integrate the dynamic equations.

B. Control

Two different control strategies are used in this paper, both described here in modal space z. First, we utilize a simple position jump to change the equilibrium position of the system from $z^- = \begin{bmatrix}0 & z_2\end{bmatrix}^T$ to another position $z^+ = \begin{bmatrix}0 & z_2 + \Delta z_2\end{bmatrix}^T$. Second, we employ a bang-bang controller similar to the one described in [19], which switches the equilibrium of the system between two positions $z = \begin{bmatrix}0 & z_2 \pm \Delta z_2\end{bmatrix}^T$ based on a torque threshold ϵ_{τ_z}.

TABLE II: Inertial and elastic parameters of the leg resulting from the optimization. Each CoM has the form $c_i^c = [0; 0; c_i]$, and each inertia has the form $I_i^c = [1, 0, 0; 0, I_i, 0; 0, 0, 1]$. Damping should be minimized while satisfying $d_1 = d_2$.

Body	Mass [10^{-3} kg]	Length [10^{-3} m]	CoM [10^{-3} m]	Inertia [10^{-6} kgm^2]
Trunk	m_t = 637			
Thigh	m_1 = 207	l_1 = 64	c_1 = 10	I_1 = 446
Shank	m_2 = 126	l_2 = 133	c_2 = 67	I_2 = 140
Foot	m_3 = 30	l_3 = 69	c_3 = 10	I_3 = 70

Elastic Parameter	Value	Unit
Spring 1	k_1 = 3.124	Nm rad^{-1}
Spring 2	$k_2 = k_1$	Nm rad^{-1}
Damping 1	$d_1 minimal$	Nms rad^{-1}
Damping 2	$d_2 = d_1$	Nms rad^{-1}

C. Simulation results

We report here in detail the simulation of the hybrid jumping system with optimal model parameters and decoupled damping. The system experiences contact losses. It incorporates a bang-bang controller to re-inject energy along the mode during the second half of the stance phase, after the lower apex. Therefore, the motion during other times of the step cycle is close to the passive dynamics of the system, as the motor position is kept constant. During limit-cycle jumping, the hybrid system exhibits no motion in polar direction, thus resulting in a pure motion on the radial mode.

V. Design of the Real Leg Prototype

For the experimental analysis of the system behavior, we built a robotic leg designed to match the specifications given in Table II. Structural parts are manufactured from PA6 by selective laser sintering (SLS). Adjustable weights are applied for fine-tuning the CoM and inertia of each segment. All active DoFs utilize ball bearings, and both kinematic constraints are realized by parallel bar mechanisms, as shown in Fig. 1: trunk to shank (in green) and thigh to foot (in black). The green trunk to shank constraint was manufactured on a different 3D printer and replaced a former belt mechanism. The electrical hardware is based on the quadrupedal DLR robot Bert [19] and uses the same power supply, main computational unit, and end-of-shaft position sensor. The leg is actuated with a newer version of the drive train including self-modified servo drives with a brushless DC motor and a four-stage spur gearbox. The servos are placed in the thigh and shank, to reinforce the idea that there is no need to reduce the leg mass for decoupling the dynamics. On the drive electronics, a low-level position controller is instantiated and commanded in cyclic synchronous position mode. The control loop between servo drive and real-time computer runs at 1 kHz, interfaced by the in-house middleware solution, Links_And_Nodes. Table III shows that the parameters of the real robotic leg are similar enough to the optimal ones. While the inertial parameters of the system match the specification well, the visco-elastic parameters deviate

from the optimum. Each DoF has 25% less stiffness than intended due to additional structural elasticities, however, the decoupling condition regarding the elastic forces is satisfied. As intended, the damping of the system is low; however, the decoupling condition $d_1 = d_2$ for the damping cannot be exactly satisfied. The CoM of the trunk is not in the hip joint, but instead on the vertical axis above it, without negatively influencing the radial oscillation mode.

VI. Experiments

In the experiments we test the modal property indicating that a deflection of the system along a mode causes a motion purely along this mode. Experiments are described and evaluated in the modal coordinates z; we focus on the radial mode described by z_2 and therefore assume the polar coordinate $z_1 = 0\,\text{rad}$. Recordings of the experiments are included in the video accompanying this paper.

A. Quantifying Modal Matching

To assess the similarity of a given system motion x to a mode described by a normalized eigenvector w it is sufficient to analyze the projection P of x onto w

$$P = \frac{1}{m}\sum_{i=1}^{m}\frac{|w^T x_i|}{\sqrt{x_i^T x_i}} \in [0,1], \tag{13}$$

with m the number of measurement points. If $P = 1$ then the evolution is a modal oscillation along w. If $P = 0$ then x is orthogonal to the mode. In our case $w = [0, 1]$. Note however that our task coordinates x have nonhomogeneous units (radians and meters). Thus, a scalar product is physically not well defined. To overcome this issue, we exploit that the relationship of joint coordinates q to the polar task coordinate x_1 is linear, as shown by (2). Thus, $x_1 = 0 \iff q_1 = -q_2$. We can therefore use P in joint space where units are homogeneous, and measure if evolutions are aligned to $[-1, 1]$. This specific property of the model lets us evaluate the radial mode in the joint space, changing (13) to

$$P^r = \frac{1}{m}\sum_{i=1}^{m}\frac{|w_q^T \bar{q}_i|}{||w_q||||\bar{q}_i||} \in [0,1], \tag{14}$$

with $w_q = [-1, 1]$ and $\bar{q}_i = q_i - q_{d,i}$.

TABLE III: System parameters of the real robotic leg. Inertia values were taken from the CAD model. The location of the segment CoMs was only roughly verified. Effective stiffness and damping of q_1 and q_2 were identified by matching the dynamics to experimental data. During the experiments the trunk mass is increased to match the value in Table II, due to the additional mass of the testbed base.

Body	Mass $[10^{-3}\,\text{kg}]$	Inertia $[10^{-6}\,\text{kgm}^2]$	Elastic Parameter		Unit
Trunk	m_t = 349		k_1 = 2.3		Nm rad^{-1}
Thigh	m_1 = 192	I_1 = 455	k_2 = 2.3		Nm rad^{-1}
Shank	m_2 = 121	I_2 = 148	d_1 = 0.0092		Nms rad^{-1}
Foot	m_3 = 30	I_3 = 71	d_2 = 0.0073		Nms rad^{-1}

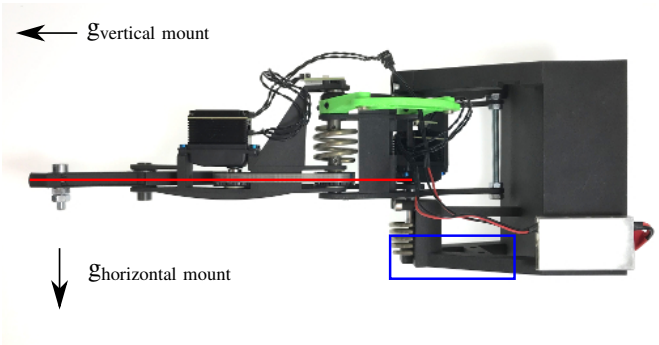

Fig. 3: Side-view of the pantograph leg. The leg moves in a plane indicated in red and is mounted to a testbed at the trunk (blue). In vertical orientation gravity is acting along the leg, whereas in horizontal orientation, gravity acts perpendicular to the motion plane.

We also define the modal coordinates as

$$z = W^{-1}q, \quad W = \begin{bmatrix} 1 & -1 \\ 1 & 1 \end{bmatrix}, \tag{15}$$

where the matrix W contains unitary eigenvectors of the linearized system at the equilibrium (for details see Section III.B and III.C of [16]). The polar mode is given by z_1, and the radial mode is given by z_2.

B. Experiments in Non-Hybrid Regimes

The behavior of the dynamic system resembling the flight and stance phase is separately evaluated. We perform experiments in three different setups, all of them restricting the number of DoFs to two.

1) Setup: The horizontal fixed-trunk setup (hFTS) aligns the motion plane of the leg horizontally (Fig. 3). This cancels out gravitational forces and therefore permits the examination of the interplay of only visco-elastic and inertial forces. Two other setups are required when applying the modal matching procedure from Section III-A. In the vertical fixed-trunk setup (vFTS), gravitational forces are aligned with the radial mode, and the foot can move freely. In the fixed-foot setup (FFS) a boom guides the trunk on a hemisphere with a large radius compared to the leg length. This approximates a planar motion, allowing free-floating movements in vertical and horizontal direction but locking rotation of the trunk for the fixed-foot experiments. The boom adds weight to the trunk such that the total system mass is 1 kg. We test the system motion in each setup for three different equilibrium positions z_2 and three different deflections Δz_2.

The system is excited through two different controllers, both based on a step input to the system. First, we command an instantaneous position jump from the initial position $z_2 + \Delta z_2$ to the target position z_2. This can be viewed as an instantaneous change of the equilibrium position of the leg, and allows to observe the passive motion of the system as a response to this step input. Second, we use a bang-bang controller to persistently inject energy into the system by switching between $z_2 \pm \Delta z_2$. This is the same controller used in simulation, which we can use to compensate for the effect of dissipative forces and reach limit-cycle motions.

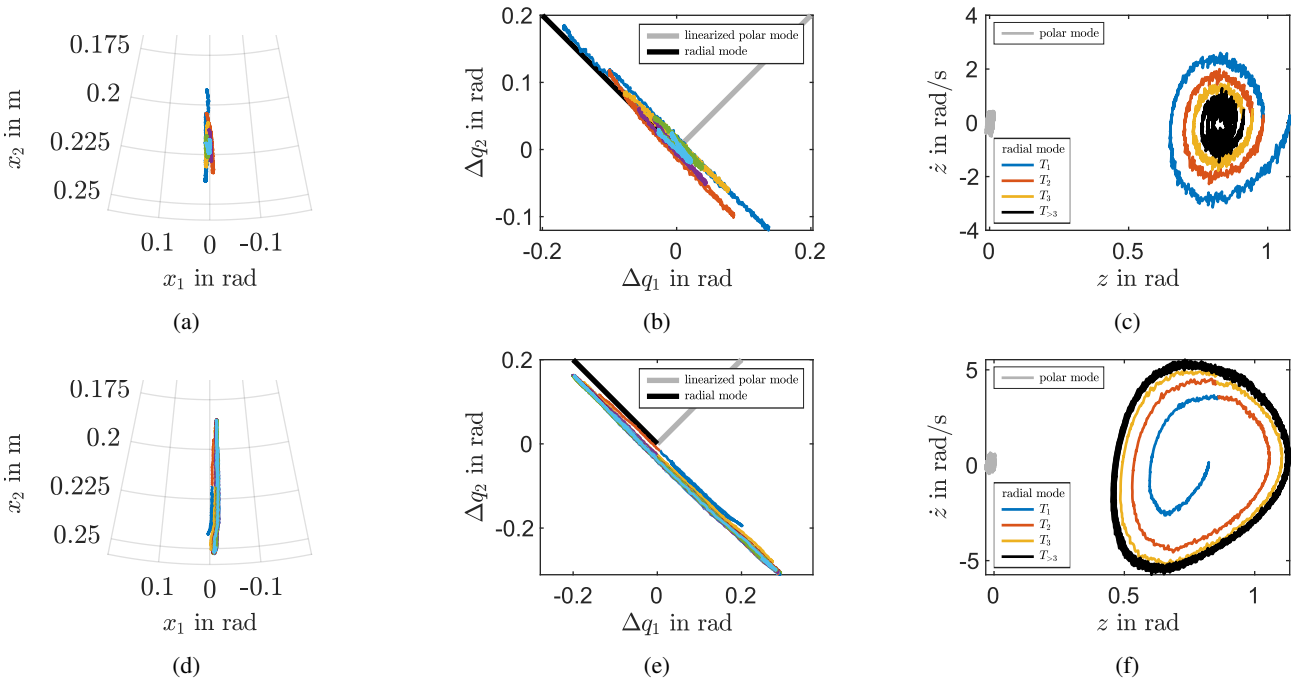

Fig. 4: Experiments performed by fixing the foot. The plots (a) - (c) show the system response to a step input from $z_2 - \Delta z_2 = 0.7$ rad to $z_2 = 1$ rad (yellow line in Fig. 5c). The plots (d) - (f) show the system response to actuation with a bang-bang controller switching between $z_2 \pm \Delta z_2 = 1.24 \pm 0.077$ rad to $z_2 = 1$ rad (yellow line in Fig. 5f). Each oscillation period is colored separately to clarify how the system moves over time. The foot tip motion w.r.t. the trunk in polar coordinates is given in (a) and (d). The corresponding motion in joint space is shown in (b) and (e), where we indicate the eigenvectors of the system, corresponding to the modal coordinates axes z. The phase plot of the system in modal coordinates is shown in (c) and (f).

2) Stance-Phase Experiments: We describe two fixed-foot experiments here in detail and resulting plots are presented in Fig. 4. In these experiments, we fixed the trunk vertically on the testbed, such that gravity was aligned with the leg. First, we commanded a step input to the system from $z_2 + \Delta z_2 = 1.7\,\text{rad}$ to $z_2 = 1.4\,\text{rad}$, which actuates the leg along the radial mode. The resulting trunk motion in polar coordinates is given in Fig. 4a, with different colors representing different oscillation periods. The perfect system motion would be a line on $x_1 = 0\,\text{rad}$. Due to the linear relationship of the polar task coordinate x_1 with the joint space q, the system motion can be compared in joint space to the eigenvector w_2 describing the radial mode (Fig. 4b). Note that the vectors $w_{1,2}$ also represent the modal coordinate axes z. As the last reference, we provide the phase plot of the experiment in the modal space (Fig. 4c), where it can be seen that the system moves with very good approximation along the radial mode. The system behavior is evaluated with (14) for each time step, averaged per period. For this specific experiment $P_1^r = 0.94$ for the first period, with a steady decline to $P_6^r = 0.78$ for the sixth period.

In the second experiment, we actuate the leg with a bang-bang controller, switching between the two equilibrium positions $z_2 \pm \Delta z_2 = 1.24\,\text{rad} \pm 0.077\,\text{rad}$. Analogous to the first experiment we provide plots of the system motion in task, joint, and phase space (Fig. 4d, 4e, 4f). When comparing the phase plots it is obvious that the step input response is a decreasing oscillation along the radial mode, whereas the bang-bang controller manages after three periods to sustain a limit-cycle oscillation with a very good mean rating of $P_{>3}^r = 0.94$.

3) Results: In Fig. 5 we report the results of over 280 experiments. It can be seen that P^r decreases with each period for the system response to a step input, independent of the chosen setup (Fig. 5a, 5b, 5c). In our particular case, the two DoFs in joint space must oscillate at the same frequency for the system to move on the radial mode. Slightly different oscillation frequencies result in growing phase shift over time, causing a decreasing rating over time. Comparing the fixed-trunk experiments, it can be seen that gravity acting along the radial mode in the vertical setup leads to an overall better rating after 6 periods. In comparison to the fixed-trunk experiments, the fixed-foot experiment rating P^r is lower. Increased inertia due to the trunk mass is a reason for a bigger discrepancy in frequencies, resulting in a bigger oscillation phase shift.

Contrary to this, the rating P^r saturates at a high value in less than ten periods for the system actuated with a bang-bang controller, independent of the chosen setup (Fig. 5d, 5e, 5f). This shows that the bang-bang controller counteracts any dissipative actions and very well sustains the system motion on a limit cycle corresponding to a strict mode. Fixed-trunk experiments with $z_2 = 1.8\,\text{rad}$ have a lower rating, indicating that not only the radial mode was excited. During these experiments with a shortened leg, we observed the foot tip moving in a circular motion instead of a line-shaped motion,

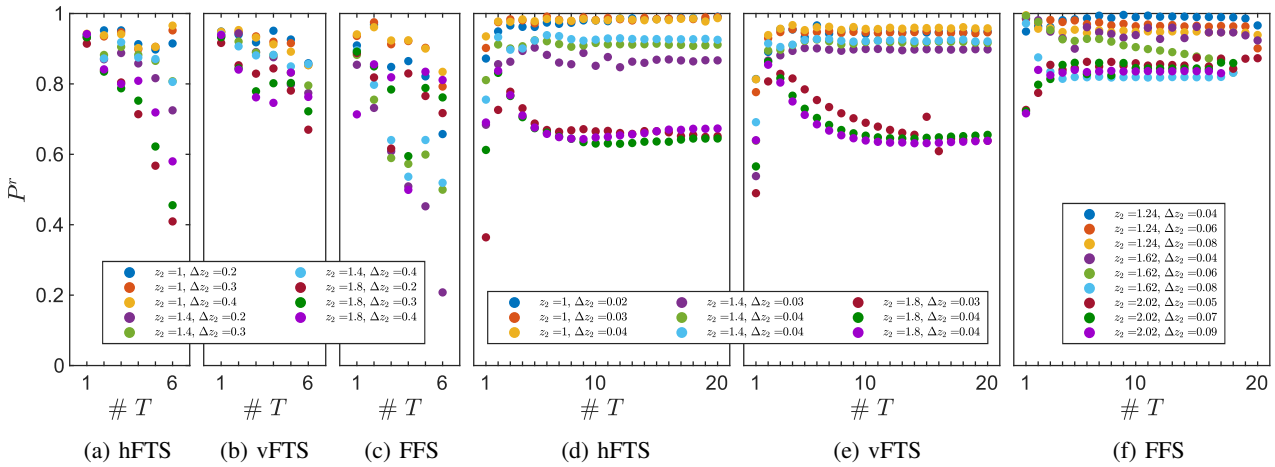

(a) hFTS (b) vFTS (c) FFS (d) hFTS (e) vFTS (f) FFS

Fig. 5: Evaluation of experiments in three different setups using (a) - (c) a single step input or (d) - (f) a bang-bang controller. The plots depict the projection P^r (13) of the system states $[q_1, q_2]$ on the **radial** mode for each oscillation period. Results of the step input response are averaged over 10 trials each (3 for the FFS). The start of each experiment was determined by the first control action. The step-input response was evaluated for oscillations larger than $0.1\Delta z_2$. The motion excited with the bang-bang controller was evaluated for the first 20 oscillation periods of an experiment of 8 seconds. z_2 and Δz_2 are given in radians.

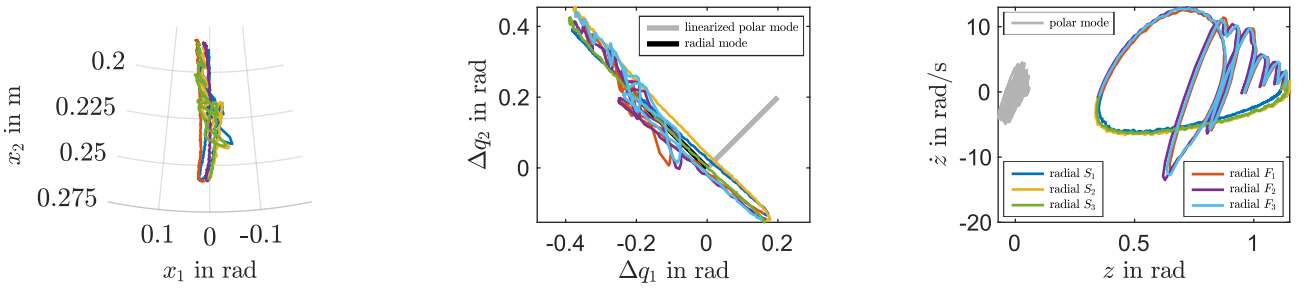

(a) (b) (c)

Fig. 6: Experiments for the hybrid jumping leg actuated with a bang-bang controller. Stance and flight phases of three jump cycles are shown in different colors to clarify how the system moves over time. The foot tip motion w.r.t. the trunk in polar coordinates is given in (a). The corresponding motion in joint space is shown in (b), where we indicate the eigenvectors of the system, corresponding to the modal coordinates axes z. The phase plot of the system in modal coordinates is shown in (c).

which points to a wrongly-tuned controller. The results show overall that the bang-bang controller manages to excite the radial mode of the system and minimizes the cross-talk effect disturbing the radial mode.

C. Jumping Oscillations in Full Hybrid Regime

Finally, we conduct a jumping experiment to assess the motion of the hybrid system jumping in place. The system is deflected by $\Delta z_2 = 0.28$ rad from its equilibrium position $z_2 = 0.8$ rad employing the aforementioned bang-bang controller. Starting from foot-ground contact, the bang-bang controller excites the system along the radial mode and injects enough energy such that the foot leaves the ground. Figure 6 reports three consecutive stance and flight phases of the system. When jumping, the system motion reaches a rating $P^r_{st} > 0.99$ for each stance phase motion, and $P^r_{fl} > 0.97$ for each flight phase.

Over the progression of three jumps the trunk moves $\Delta x_t = 0.018$m in horizontal direction, opposed to $\Delta z_t = 0.085$m in vertical direction, again showing that the motion in the radial direction is prevalent. During the flight phase, the foot reaches a height of $z_f = 0.045$m, with horizontal movement of $\Delta x_f = 0.025$m. Figure 7 presents snapshots of one jump of the leg.

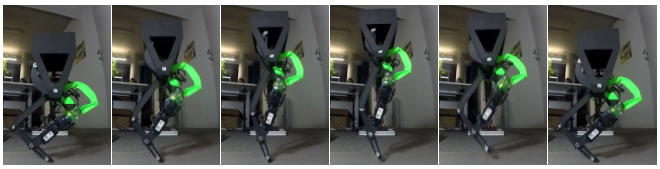

Fig. 7: A series of stills taken from a video of the jumping experiment, showing one jump from lower apex to consecutive lower apex.

VII. Conclusion

In this paper, we investigate the embodiment of SLIP-like dynamics into a segmented robotic leg by means of implementing a strict mode along the radial task coordinate. This has been obtained by shaping at the same time the

elastic potential and the mass distribution of each rigid body involved. Based on this design we built a prototype of the leg, which was used in over 280 experiments. We tested the modal property in different configurations and operation modes of the robot. In all experiments, we could show that the system mainly moves along the radial strict mode, independent of robot configuration and control strategy. With these experiments, we provide proof of the existence of the designed strict mode in the leg dynamics.

This paper brings us closer to our vision of template-based near-passive robotic locomotion through the embodiment of oscillatory modes. Yet, to get there substantial research effort is still needed. Future work will be focused on characterizing the polar motion of the leg, as well as the corresponding oscillatory mode. We will direct efforts towards implementing locomotion gaits that exploit the passive dynamic leg swing on a quadrupedal system built by combining four of the proposed legs.

ACKNOWLEDGMENT

The authors would like to thank Thomas Gumpert, Annika Schmidt, Daniel Seidel, and Philipp Stratmann for ongoing software and hardware support as well as infrastructural work for the robotic leg.

APPENDIX I
RIGID BODY DYNAMICS IN STANCE

$$
\begin{aligned}
t_1 &= (m_t + m_1)l_1 - c_1 m_1 \\
t_2 &= (m_t + m_1 + m_2)(l_1 + l_3) - c_2 m_2 \\
t_3 &= (m_t + m_1 + m_2 + m_3)l_3 - c_3 m_3 \\
t_4 &= t_1(l_1 + l_3) + t_2 l_3 \\
t_5 &= (t_1 - c_1 m_1)l_1 + m_1 c_1^2 + I_1 \\
t_6 &= (t_2 - c_2 m_2)(l_1 + l_3) + m_2 c_2^2 + I_2 \\
t_7 &= (t_3 - c_3 m_3)l_3 + m_3 c_3^2 + I_3
\end{aligned}
$$

$$
M(q) = \begin{bmatrix} 2t_1 l_3 + t_5 + t_7 & \cos(q_1 - q_2)t_4 \\ \cos(q_1 - q_2)t_4 & t_6 \end{bmatrix} \tag{16}
$$

$$
C(q, \dot{q}) = \begin{bmatrix} 0 & \dot{q}_2 \sin(q_1 - q_2)t_4 \\ -\dot{q}_1 \sin(q_1 - q_2)t_4 & 0 \end{bmatrix} \tag{17}
$$

$$
g(q) = \begin{bmatrix} -g0 \sin(q_1)(t_1 + t_3) \\ -g0 \sin(q_2)t_2 \end{bmatrix} \tag{18}
$$

APPENDIX II
DETAILED DECOUPLING OF THE TASK INERTIA

The inverse of the Jacobian $J(q) = \partial x / \partial [q_1, q_2]$ is

$$
J^{-1}(q) = \begin{bmatrix} 1 & -t_8 \\ 1 & t_8 \end{bmatrix}, t_8 = \frac{\sqrt{2 + 2\cos(q_1 - q_2)}}{2(l_1 + l_3)\sin(q_1 - q_2)}. \tag{19}
$$

The task space inertia matrix $M_x = J(q)^{-T} M(q) J(q)^{-1}$ is then decoupled if (20) is solved, which is equal to (5).

$$
\begin{aligned}
0 &= [0\ 1]\, M_x\, [1\ 0]^T \\
&= \left([0\ 1]\, J(q)^{-T}\right)\, M(q)\, \left(J(q)^{-1}\, [1\ 0]^T\right) \\
&= [-t_8\ t_8]\, M(q)\, [1\ 1]^T \\
&= -t_8(2t_1 l_3 + t_5 + t_7 - t_6)
\end{aligned} \tag{20}
$$

REFERENCES

[1] C. Schumacher, M. Sharbafi, A. Seyfarth, and C. Rode, "Biarticular muscles in light of template models, experiments and robotics: a review," *J. of the Royal Society Interface*, vol. 17, no. 163, p. 20180413, 2020.

[2] C. Della Santina, M. G. Catalano, and A. Bicchi, "Soft robots," *Encyclopedia of Robotics*, 2020.

[3] M. Calisti, G. Picardi, and C. Laschi, "Fundamentals of soft robot locomotion," *J. of The Royal Society Interface*, vol. 14, no. 130, p. 20170101, 2017.

[4] M. A. Sharbafi, M. J. Yazdanpanah, M. N. Ahmadabadi, and A. Seyfarth, "Parallel compliance design for increasing robustness and efficiency in legged locomotion-theoretical background and applications," *IEEE/ASME Trans. on Mechatronics*, 2020.

[5] Z. Gan, Y. Yesilevskiy, P. Zaytsev, and C. D. Remy, "All common bipedal gaits emerge from a single passive model," *J. of The Royal Society Interface*, vol. 15, no. 146, p. 20180455, 2018.

[6] A. Abate, R. L. Hatton, and J. Hurst, "Passive-dynamic leg design for agile robots," in *IEEE Int. Conf. on robotics and automation (ICRA)*, 2015, pp. 4519–4524.

[7] M. H. Raibert, H. B. Brown Jr, and M. Chepponis, "Experiments in balance with a 3D one-legged hopping machine," *Int. J. of Robotics Research*, vol. 3, no. 2, pp. 75–92, 1984.

[8] H. Shin, T. Ishikawa, T. Kamioka, K. Hosoda, and T. Yoshiike, "Mechanistic properties of five-bar parallel mechanism for leg structure based on spring loaded inverted pendulum," in *IEEE-RAS Int. Conf. on Humanoid Robots*, 2019, pp. 320–327.

[9] S. Rezazadeh and J. W. Hurst, "Control of ATRIAS in three dimensions: Walking as a forced-oscillation problem," *Int. J. of Robotics Research*, vol. 39, no. 7, pp. 774–796, 2020.

[10] A. Spröwitz, A. Tuleu, M. Vespignani, M. Ajallooeian, E. Badri, and A. Ijspeert, "Towards dynamic trot gait locomotion: Design, control, and experiments with Cheetah-cub, a compliant quadruped robot," *Int. J. of Robotics Research*, vol. 32, no. 8, pp. 932–950, 2013.

[11] B. Katz, J. Di Carlo, and S. Kim, "Mini Cheetah: A platform for pushing the limits of dynamic quadruped control," in *IEEE Int. Conf. on Robotics and Automation (ICRA)*, 2019, pp. 6295–6301.

[12] K. Green, Y. Godse, J. Dao, R. L. Hatton, A. Fern, and J. Hurst, "Learning spring mass locomotion: Guiding policies with a reduced-order model," *IEEE Robotics and Automation Letters*, vol. 6, no. 2, pp. 3926–3932, 2021.

[13] P. Arm, R. Zenkl, P. Barton, L. Beglinger, A. Dietsche, L. Ferrazzini, *et al.*, "Spacebok: A dynamic legged robot for space exploration," in *Int. Conf. on Robotics and Automation (ICRA)*, 2019, pp. 6288–6294.

[14] A. Albu-Schäffer and C. Della Santina, "A review on nonlinear modes in conservative mechanical systems," *Annual Reviews in Control*, 2020.

[15] A. Albu-Schäffer, D. Lakatos, and S. Stramigioli, "Strict nonlinear normal modes of systems characterized by scalar functions on riemannian manifolds," *IEEE Robotics and Automation Letters*, pp. 1–1, 2021.

[16] D. Lakatos, W. Friedl, and A. Albu-Schäffer, "Eigenmodes of nonlinear dynamics: Definition, existence, and embodiment into legged robots with elastic elements," *IEEE Robotics and Automation Letters*, vol. 2, no. 2, pp. 1062–1069, 2017.

[17] C. T. Farley, J. Glasheen, and T. A. McMahon, "Running springs: speed and animal size," *J. of experimental Biology*, vol. 185, no. 1, pp. 71–86, 1993.

[18] B. M. Kilbourne and L. C. Hoffman, "Scale effects between body size and limb design in quadrupedal mammals," *PloS one*, vol. 8, no. 11, p. e78392, 2013.

[19] D. Lakatos, K. Ploeger, F. Loeffl, D. Seidel, F. Schmidt, T. Gumpert, F. John, T. Bertram, and A. Albu-Schäffer, "Dynamic locomotion gaits of a compliantly actuated quadruped with slip-like articulated legs embodied in the mechanical design," *IEEE Robotics and Automation Letters*, vol. 3, no. 4, pp. 3908–3915, 2018.

[20] D. Calzolari, C. Della Santina, and A. Albu-Schäffer, "PD-like regulation of mechanical systems with prescribed bounds of exponential stability: the point-to-point case," *IEEE Control Systems Letters*, 2020.

[21] D. Molina, A. LaTorre, and F. Herrera, "An insight into bio-inspired and evolutionary algorithms for global optimization: review, analysis, and lessons learnt over a decade of competitions," *Cognitive Computation*, vol. 10, no. 4, pp. 517–544, 2018.